Semiclassical analysis of angular differential cross sections for single-electron capture in 250-eV $H^+ + H$ collisions

F. Frémont*

Université de Caen, CIMAP, 6, Boulevard du Maréchal Juin, 14050 Caen Cedex, France

(Received 16 April 2015; published 27 May 2015)

A classical model based on the resolution of Hamilton equations of motion is used to determine the angular distribution of H projectiles following single-electron capture in $H^+ + H$ collisions at an incident projectile energy of 250 eV. At such low energies, the experimental charge-exchange probability and angular differential cross sections exhibit oscillatory structures that are classically related to the number of swaps the electron experiences between the target and the projectile during the collision. These oscillations are well reproduced by models based on quantum mechanics. In the present paper, the angular distribution of H projectiles is determined classically, at angles varying from 0.1° up to 7°. The variation in intensity due to interferences caused by the indiscernibility between different trajectories is calculated, and the role of these interferences is discussed.

DOI: 10.1103/PhysRevA.91.052709 PACS number(s): 34.70.+e, 34.50.−s, 34.10.+x

I. INTRODUCTION

For many decades, electron capture in ion-atom collisions has been extensively studied. In particular, the collision system $H^+ + H$ has received a great deal of attention, experimentally [1–4] and theoretically [5–11], since it is the simplest resonant system involving two centers and an active electron.

The process to study is written

$$H^+ + H(1s) \rightarrow H^*(n) + H^+ \quad (1)$$

where the projectile is, after electron capture, mainly in the fundamental state ($n = 1$), or in an excited state ($n \geqslant 2$).

Total capture cross sections σ_{SC} have been determined experimentally with a relative uncertainty of less than 10%, in a large range of projectile energies (1 keV–10 MeV). From a theoretical point of view, various models based on quantum mechanics reproduce the experiment very well [10,12]. Classical methods have also been used to calculate σ_{SC}. At projectile energies larger than 30 keV, calculations agree well with experiment [13]. At energies smaller than 30 keV, calculated cross sections remain constant and are of the order of 3×10^{-16} cm^2, while experimental cross sections increase slowly with decreasing projectile energy, to reach $\sim1.5\times10^{-16}$ cm^2 at 1 keV. The discrepancy observed at low energies is due to several effects, despite improved calculations that describe the quantum electronic density by means of phase-space distributions, such as the well-known Wigner distribution [14]. One of the most important effects has been discussed in detail a few years ago [11]. At very low energies, oscillatory structures have been evidenced in the impact velocity distribution of the capture probability [4]. Similar oscillations also appear in the impact parameter distribution, as well as in the projectile scattering angle distribution. On a quantum point of view, these oscillations have been interpreted in terms of interferences between the main capture and the elastic scattering channels. Classically, these oscillations were interpreted in terms of swaps of the electron between the target and the projectile nuclear centers [11]. When calculations are performed in one dimension, the classical trajectory Monte Carlo (CTMC) calculations are able to reproduce the quantum oscillatory behavior of the probability. However, three-dimensional (3D) CTMC calculations fail to reproduce the quantum calculations. Indeed, the classical probability is of the order of 0.5 in the projectile energy range 0.05–1 keV, and the small deviations of the probability are due, according to the authors, to statistical uncertainties rather than collisional effects [11].

In the present work, the $H^+ + H$ collision system is revisited for an impact energy of 250 eV. Instead of capture probability, that has been already studied, we focus attention on the angular distribution of H atoms after electron capture. First, in addition to Coulomb potentials between the electron and the nuclei, a phenomenological potential V_H is included, in order to simulate the Heisenberg uncertainty principle. This potential, introduced many years ago in nuclear physics [15], and then in atomic physics [16–18], has been used to mimic the shell structure of many-electron atoms or molecules and to avoid either the electrons collapsing onto the nucleus, or autoionizing. Second, since interferences play a major role at low impact energy, interferences caused by H atoms that reach the detector at a given detection angle θ_d are taken into account in the calculation. Very recently, a model was constructed, based on the corpuscular aspect and then on the wave behavior of electrons, to describe interferences phenomena observed experimentally in the angular distribution of Auger electrons following double electron capture in 30-keV $He^{2+} + H_2$ collisions [19]. The model was able to reproduce, qualitatively and quantitatively, the experimental results.

In Sec. II, the model is presented. The method used to represent the collision itself is first described. Since the way to determine interference contributions has been written in detail previously, only a brief description is made here. In Sec. III, calculated angular distributions are shown, and compared, after normalization, with previous experimental and calculated results. The role of interferences is discussed.

II. SEMICLASSICAL MODEL

A. Description of the collision

The total Hamiltonian is written (atomic units are used)

$$H = \sum_{i=1}^{2} \frac{p_i^2}{2M} + \frac{p_e^2}{2} - \sum_{i=1}^{2} \frac{1}{\|\vec{r}_i - \vec{r}_e\|} + \frac{1}{\|\vec{r}_1 - \vec{r}_2\|} + \sum_{i=1}^{2} V_{Hi}. \quad (2)$$

*francois.fremont@ensicaen.fr

In the above expression, $\vec{p}_i$ and $\vec{p}_e$ are the momenta of the protons and the electron, respectively, M is the proton mass, and $\vec{r}_i$ and $\vec{r}_e$ characterize the respective positions of the protons and the electron in the laboratory frame. The repulsive potential $V_{\mathrm{H}i}$ between the electron and one proton is of the form [20]

$$V_{\mathrm{H}i} = \frac{\xi_{\mathrm{H}}^2}{4\alpha\mu r_{ie}^2} \exp\left\{\alpha\left[1 - \left(\frac{r_{ie}p_{ie}}{\xi_{\mathrm{H}}}\right)^4\right]\right\}. \quad (3)$$

In this expression, i refers to the H^+ target or projectile, ξ_{H} and α are adjustable parameters, and μ is the reduced mass of the electron-proton system. The quantities r_{ie} and p_{ie} are the relative positions and momenta [20]. The parameters ξ_{H} and α are chosen [16] so that the final electron energy on the H atom is close to 0.5 a.u. Values for ξ_{H} and α are found to be 0.9582 and 4, respectively [20]. Due to this constraint, final momentum and position distributions of the bound electron do not resemble the quantum distributions.

The time evolution of the system is given by the following coupled equations:

$$\frac{dp_{i\alpha}}{dt} = -\frac{\partial H}{dr_{i\alpha}}, \quad \frac{dr_{i\alpha}}{dt} = \frac{\partial H}{dp_{i\alpha}}, \quad (4)$$

where i refers to the three moving particles, and α indicates the three components of the vectors along the three coordinate axes.

At $t = 0$, the projectile is at a distance $z_p = -500$ a.u. [the (Oz) axis is parallel to the incident beam direction], and the orientation of the electron around the target is randomly chosen. The impact parameter b varies from 0 to 8 a.u., and the angle φ_p which characterizes the position of the projectile in the (xOy) plane, perpendicular to (Oz), is also randomly chosen. From the initial conditions, the Hamiltonian equations (4) are numerically solved using the Runge-Kutta method of order 4, with an adaptive step defined and described in Ref. [6]. At the end of the collision, the number of H projectiles that have captured the target electron is determined as a function of the scattering angle θ_p. To obtain good statistics, the number of calculated trajectories was fixed to 500 000. Integration time was chosen as follows: Let us call θ_P^v and θ_P^r the angles between the incident beam direction and the final atom velocity $\vec{V}_P$ and position $\vec{r}_P$, respectively; calculation was ended when the condition $\theta_P^v - \theta_P^r < 0.1^\circ$ was fulfilled (see Fig. 4 of Ref. [19]). This condition corresponds to an integration time $t_{\max}$ of the order of 3000 a.u.

B. Determination of the phase shift

The method to calculate phase shifts due to interferences between different trajectories is similar to that described in Ref. [18], so that only a brief description is given here. Suppose two H atoms reach the detector at times t_1 and t_2 ($t_1 < t_2$). The latter is therefore delayed compared to the first atom, and the missing distance for the second atom to reach the detector is δ_{12}, which is easily calculated as a function of the coordinates and the final angles [18].

The probability that a electron is emitted by Auger effect is equal to unity. Thus, the amplitude associated with a H atom i is

$$A_i(\theta_P) = e^{-iE_i\left(t_{\max} - \frac{\delta_{1i}}{v_i}\right)}, \quad (5)$$

where E_i is the electron kinetic energy, v_i is the projectile velocity at the end of the collision, and δ_{1i}/v_i is the phase shift induced by the delay. The total amplitude $A(\theta_d)$ at a fixed angle $\theta_P \pm \Delta\theta_P$, where $\Delta\theta_P \sim 0.1$ deg is the experimental angular resolution [4], is the sum of the individual amplitudes A_i. Finally, the intensity is determined using $I(\theta_P) = |A(\theta_P)|^2 = |\sum_i A_i(\theta_P)|^2$.

III. ANGULAR DISTRIBUTION OF H ATOMS

A. Results of the calculation

Figure 1 shows the impact parameter distribution $d\sigma_C/db$ of H atoms after electron capture. This distribution is defined by

$$\frac{d\sigma_C}{db} = 2\pi b P_c(b), \quad (6)$$

where $P_c(b)$ is the capture probability at a given impact parameter. The distribution is maximum at $b \sim 3$ a.u., which is coherent with previous calculations performed at higher projectile energies [21], but smaller than the value of ~4 a.u. obtained at 500 eV [22]. As expected [11], no oscillation is seen.

The total capture cross section σ_C, obtained by integration of $d\sigma_C/db$ over all the range of impact parameters, is $\sim 8.9\times10^{-16}$ cm^2, which is smaller than the expected cross section of about 3×10^{-15} cm^2 evaluated by extrapolation of previous experimental cross sections [2].

To determine the differential cross section $d\sigma_C/d\Omega$, where $d\Omega$ is the solid angle as viewed by the detector, it is necessary to know $d\Omega$, defined by $d\Omega = 2\pi \sin\theta_P d\theta_P$ as a function of the impact parameter. Figure 2 shows the dependence of b with θ_P, resulting from the present calculation.

In contrast with what happens in a two-body problem, there is no biunivocal relation between the two quantities

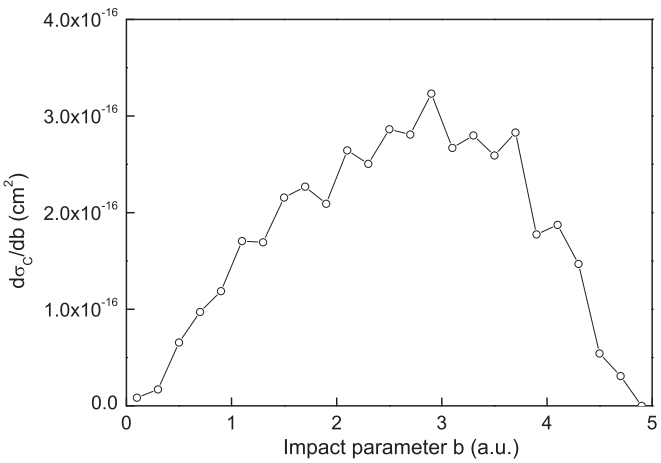

FIG. 1. Calculated differential cross section $d\sigma_C/db$ as a function of the impact parameter b following electron capture in 250-eV H^+ + H collisions. The total capture cross section is obtained by integration of $d\sigma_C/db$ over b.

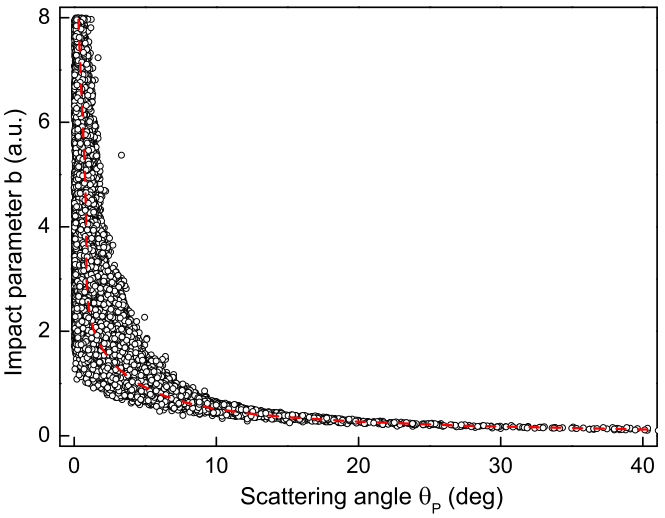

FIG. 2. (Color online) Impact parameter b as a function of projectile scattering angle θ_P (open circles), calculated for 250-eV $H^+ + H$ collisions. The red dashed curve is the result of the calculation in two-body collisions.

(a biunivocal relation would give rise to the red dashed curve shown in Fig. 2). As an example, for $\theta_P = 4$ deg, b varies from 0.63 a.u. up to 1.6 a.u. Therefore, the well-known formula $\frac{d\sigma_C}{d\Omega} = \frac{b}{\sin\theta_P}|\frac{db}{d\theta_P}|$ cannot be used, because the quantity $db/d\Omega$ is not defined.

Hence b has to be replaced, at a given detection angle θ_d, by an impact parameter distribution $f(b) = N_C(b)/N_{\rm tot}(b)$, where $N_C(b)$ is the number of captured electrons and $N_{\rm tot}(b)$ is the total number of electrons involved in the collision. Finally, the differential cross section becomes

$$\frac{d\sigma_C}{d\Omega} = \frac{1}{\sin\theta_P d\theta_P}\int bf\,(b)\,db. \qquad (7)$$

In this expression, for a given value of θ_P, b varies from $b_{\rm min}$ to $b_{\rm max}$.

The classical results for $d\sigma_C/d\Omega$ are presented in Fig. 3 for scattering angles varying from 0.05° up to 7°. In Figs. 3(a) and 3(b), the dashed black curve is the result of the calculation if the relation $\frac{d\sigma_C}{d\Omega} = \frac{b}{\sin\theta_P}|\frac{db}{d\theta_P}|$ is used. The blue squares in Fig. 3(a) result from the classical calculation using relation (7). In contrast with the previous curve, series of maxima, depicted by blue arrows, and minima are visible, and located at scattering angles of about 1°, 2.4°, 4°, and 5°. It is noted that the presence of maxima and minima is not due to a lack of statistics, except at angles larger than ∼5.5°. As a first conclusion, to get evidence for oscillations, observed by smoothing the calculation (blue curve), taking into account the impact parameter distribution is found to be necessary.

When interferences between capture pathways are introduced, by applying the method described in Sec. II B and also in details in Ref. [19], the oscillations are also observed [red squares in Fig. 3(b)], with a larger amplitude than that observed in Fig. 3(a). Series of maxima and minima are now clearly evidenced [red arrows in Fig. 3(b)]. In addition to maxima located at 1°, 2°, 4°, and 5°, an additional maximum is seen at ∼0.5°.

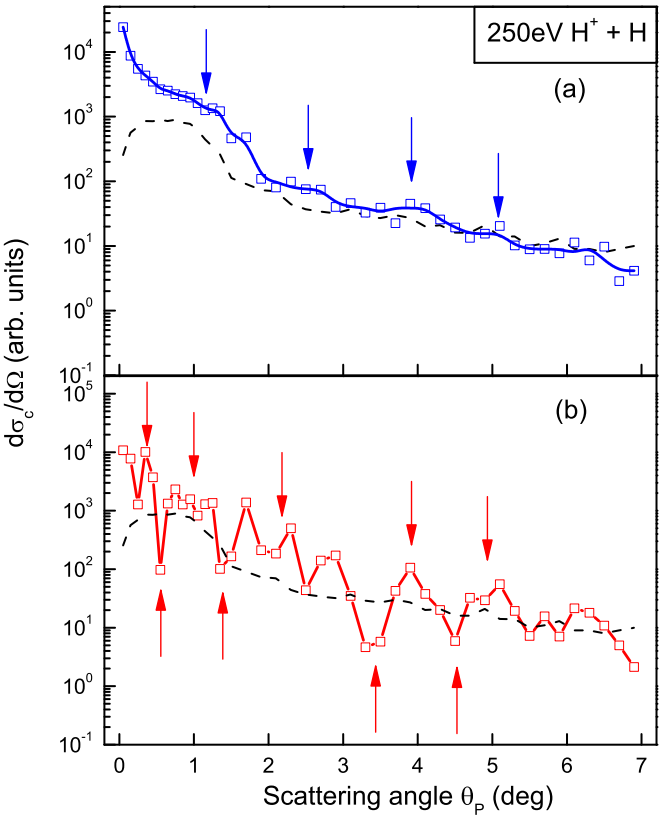

FIG. 3. (Color online) Differential cross section $d\sigma_C/d\Omega$ as a function of the scattering angle θ_P calculated with the present model. Dashed line: calculation using the simple formula $\frac{d\sigma_C}{d\Omega} = \frac{b}{\sin\theta_P}|\frac{db}{d\theta_P}|$; blue curve and open squares: calculation using relation (7), without inclusion of interferences; red curve and open squares: calculation using relation (7) including interferences.

B. Comparison with previous experimental and theoretical results

To go further in the details of the present analysis, our results have to be compared with existing experimental and theoretical results. In Figs. 4(a) and 4(c), experimental angular distribution is represented (full black circles and short-dashed curve) for angles ranging from 1.5° to 7° [4]. The cross section oscillates, and maxima are located at ∼2.5° and 4.2°. Theoretical angular distributions originating from quantum mechanics [23] are shown in Figs. 4(b) and 4(d) (empty circles and dashed curves). The theory gives evidence for strong series of maxima and minima. It is noted that the blue curve is normalized to experiment at the arbitrary angle of 1.5°.

We first focus our attention on the present calculation that neglects the interferences between the capture pathways (blue curve on the left side of Fig. 4). The slope of the curve is in good agreement with experiment. Moreover, the position of the maxima (2.5°, 4.2°), as well as the amplitude of the oscillations, are coherent with that found experimentally. In contrast, the oscillation amplitude originating from the classical calculation is much smaller than that found with the quantum mechanics model. This result is not surprising since the latter model takes into account the interferences. Despite the dramatic difference

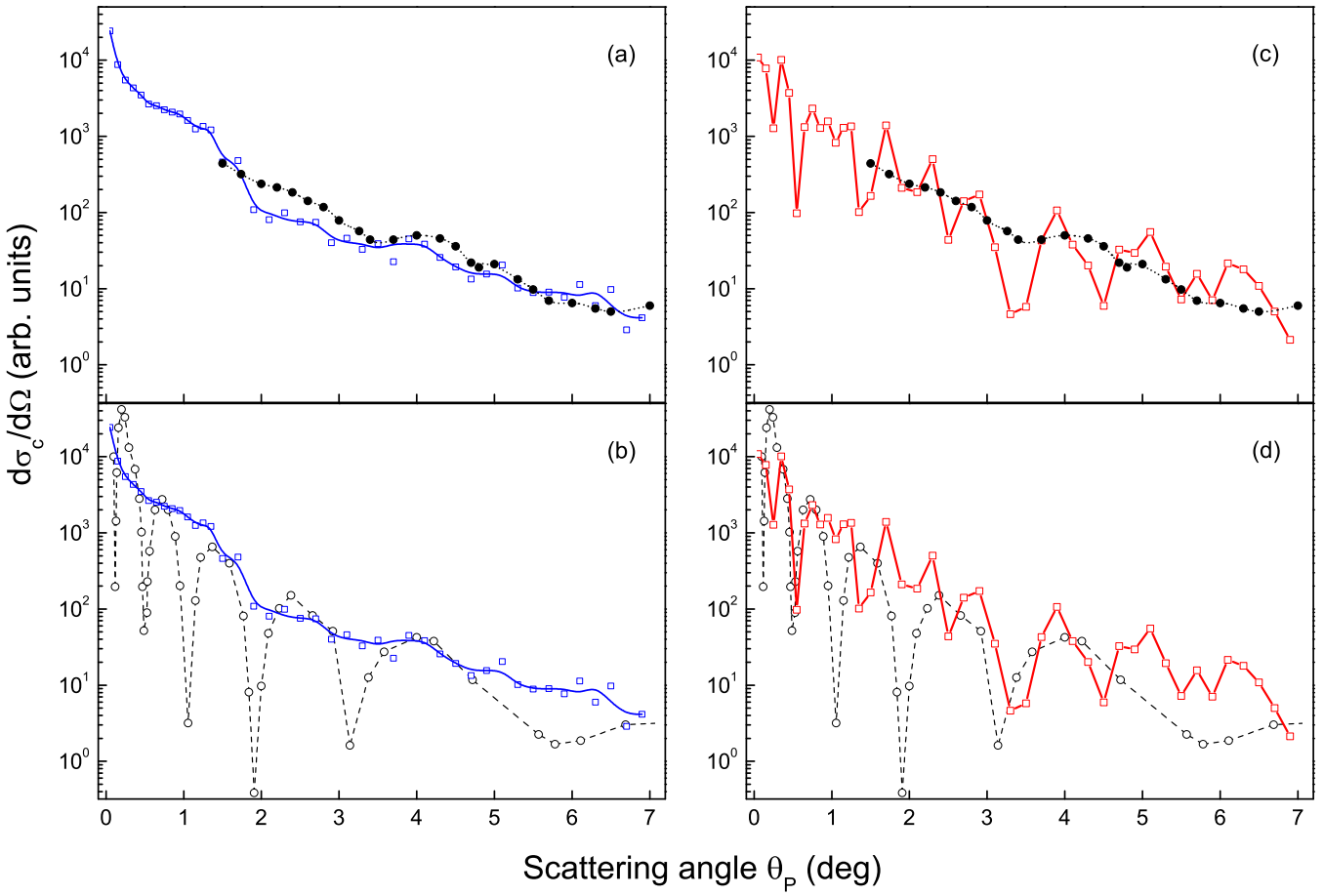

FIG. 4. (Color online) Differential cross section $d\sigma_C/d\Omega$ as a function of the scattering angle θ_P. Blue curve and open squares: calculation using relation (7), without inclusion of interferences (a, b); red curve and open squares: calculation using relation (7) including interferences (c, d). The present results are compared to previous experiment [4] and quantum calculation [23].

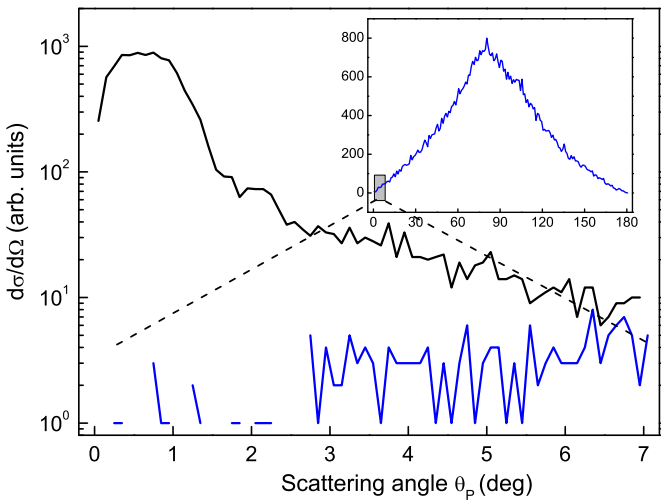

FIG. 5. (Color online) Differential cross section $d\sigma_C/d\Omega$ as a function of the scattering angle θ_P, calculated with the present model, for electron capture (black curve) and elastic scattering (blue curve). The angular range is 0°–7°. The cross section for electron capture is calculated with the simple formula $\frac{d\sigma_C}{d\Omega} = \frac{b}{\sin\theta_P}|\frac{db}{d\theta_P}|$.

between both calculations, the position of the maxima is found to be similar in both cases, except when θ_d is larger than 4.5°.

When interferences are included in our calculations, surprisingly, the agreement is better when comparing with the quantum calculation [Fig. 4(d)]. Again, the slopes of both curves are close to each other. In addition, some maxima and minima coincide remarkably well, especially at angles smaller than 1° and between 2.5° and 4.5°. While discrepancies exist, the amplitudes of the oscillations are of the same order of magnitude, except at angles larger than 5°.

At present, only capture transitions have been taken into account to determine interference pattern. In principle, one would have to also incorporate direct scattering. However, as seen in Fig. 5, the number of events that contribute to direct scattering is maximum at angles close to 80° (inset in Fig. 5), but much smaller than that to electron capture at angles smaller than 7°. Therefore, the role of direct scattering on the interference pattern is expected to be negligible.

IV. CONCLUSION

A three-body classical model has been developed and applied to discuss the role of interferences in 250-eV $H^+ + H$ collisions. First, total capture cross section has been

determined, and is found to be smaller than the recommended cross section by a factor of ∼3. Then, differential cross section $d\sigma_C/d\Omega$ for electron capture has been calculated, including (or not) interferences, and compared with previous experiment [4] and theoretical results based on quantum mechanics [23]. In contrast with impact parameter distribution, angular distribution clearly exhibits oscillations, whose amplitude increases when interferences are taken into account. Surprisingly, while the absence of interferences in the calculations gives rise to cross sections that are very similar to that found experimentally, the inclusion of interferences fails to reproduce the experiment, but is in qualitative agreement with the quantum theory.

Therefore, the interpretation of oscillations in the angular distribution of H atoms following electron capture is questionable. Classically, the oscillations are related to the number of swaps the electron experiences between the target and the projectile centers during the collision. In quantum mechanics, the oscillations originate from the interference of two different collisional paths. Both interpretations, in view of our calculations, are reasonable.

For a deeper understanding of the phenomenon, more calculations would be necessary. In particular, analysis of the evolution of the angular distribution with the projectile velocity is required.

ACKNOWLEDGMENTS

The author is grateful to Professor C. Dufour (CIMAP, Caen) and Professor O. Juillet (LPC, Caen) for helpful discussions about analogies between classical and quantum interpretations.

[1] C. F. Barnett and H. K. Reynolds, Phys. Rev. **109**, 355 (1958).
[2] W. L. Fite, R. F. Stebbings, D. G. Hummerp, and R. T. Brackmann, Phys. Rev. **119**, 663 (1960).
[3] G. W. McClure, Phys. Rev. **148**, 47 (1966).
[4] J. C. Houver, J. Fayeton, and M. Barat, J. Phys. B: At. Mol. Phys. **7**, 1358 (1974).
[5] I. M. Cheshire, Phys. Rev. **138**, A992 (1965).
[6] R. Abrines and I. Percival, Proc. Phys. Soc. **88**, 861 (1966).
[7] S. K. Knudson and W. R. Thorson, Can. J. Phys. **48**, 313 (1970).
[8] R. McCarroll and R. D. Piacentini, J. Phys. B: At. Mol. Phys. **3**, 1336 (1970).
[9] D. J. W. Hardie and R. E. Olson, J. Phys. B: At. Mol. Phys. **16**, 1983 (1983).
[10] L. F. Errea, C. Harel, C. Illescas, H. Jouin, L. Mendez, B. Pons, and A Riera, J. Phys. B: At. Mol. Phys. **31**, 3199 (1998).
[11] P. Botheron and B. Pons, Phys. Rev. A **83**, 062704 (2011)
[12] E. O. Alt, A. S. Kadyrov, and A. M. Mukhamedzhanov, Phys. Rev. A **60**, 314 (1999).
[13] R. E. Olson and A. Salop, Phys. Rev. A **16**, 531 (1977).
[14] E. P. Wigner, Phys. Rev. **40**, 749 (1932).
[15] L. Wilets, E. M. Henley, M. Kraft, and A. D. Mackellar, Nucl. Phys. A **282**, 341 (1977).
[16] C. L. Kirschbaum and L. Wilets, Phys. Rev. A **21**, 834 (1980).
[17] J. S. Cohen, Phys. Rev. A **51**, 266 (1995).
[18] A. Dubois, J. Caillat, J. P. Hansen, I. Sundvor, F. Frémont, P. Sobocinski, J.-Y. Chesnel, R. Gayet, J. Fu, M. J. Fitzpatrick, W. F. Smith, and J. F. Reading, Nucl. Instrum. Methods Phys. Res., Sect. B **241**, 48 (2005).
[19] G. Oliviéro, V. Pestel, L. Bottey, M. Philippe, and F. Frémont, Phys. Rev. A **90**, 042711 (2014).
[20] J. S. Cohen, Phys. Rev. A **54**, 573 (1996).
[21] D. Eichenauer, N. Grun, and W. Scheid, J. Phys. B: At. Mol. Phys. **14**, 3929 (1981).
[22] R. Longo, E. Deumens, and Y. Öhrn, J. Chem. Phys. **99**, 4554 (1993).
[23] B. J. Killian, R. Cabrera-Trujillo, E. Deumens, and Y. Öhrn, J. Phys. B: At. Mol. Phys. **37**, 4733 (2004).